Missouri University of Science and Technology
Scholars' Mine

Chemistry Faculty Research & Creative Works | Chemistry

01 Jul 1982

Binary Collision Dynamics and Numerical Evaluation of Dilute Gas Transport Properties for Potentials with Multiple Extrema

James C. Rainwater

Paul M. Holland

Louis Biolsi
Missouri University of Science and Technology, biolsi@mst.edu

Follow this and additional works at: https://scholarsmine.mst.edu/chem_facwork

Part of the Chemistry Commons

Recommended Citation

J. C. Rainwater et al., "Binary Collision Dynamics and Numerical Evaluation of Dilute Gas Transport Properties for Potentials with Multiple Extrema," *Journal of Chemical Physics*, vol. 77, no. 1, pp. 434-447, American Institute of Physics (AIP), Jul 1982.
The definitive version is available at https://doi.org/10.1063/1.443625

This Article - Journal is brought to you for free and open access by Scholars' Mine. It has been accepted for inclusion in Chemistry Faculty Research & Creative Works by an authorized administrator of Scholars' Mine. This work is protected by U. S. Copyright Law. Unauthorized use including reproduction for redistribution requires the permission of the copyright holder. For more information, please contact scholarsmine@mst.edu.

Binary collision dynamics and numerical evaluation of dilute gas transport properties for potentials with multiple extrema[a)b)]

James C. Rainwater

Thermophysical Properties Division, National Engineering Laboratory, National Bureau of Standards, Boulder, Colorado 80303

Paul M. Holland[c)]

Cooperative Institute for Research in Environmental Sciences, University of Colorado/NOAA, Boulder, Colorado 80309

Louis Biolsi

Chemistry Department, University of Missouri-Rolla, Rolla, Missouri 65401
(Received 18 January 1982; accepted 11 March 1982)

Prediction of gaseous transport properties requires calculation of Chapman–Enskog collision integrals which depend on all possible binary collision trajectories. The interparticle potential is required as input, and for a variety of applications involving monatomic gases the Hulburt–Hirschfelder potential is useful since it is determined entirely from spectroscopic information and can accomodate the long-range maxima and minima found in many systems. Hulburt–Hirschfelder potentials are classified into five distinct types according to their qualitative binary collision dynamics, which in general can be quite complex and can exhibit "double orbiting", i.e., a pair of orbiting impact parameters for a single energy of collision. The collision integral program of O'Hara and Smith has been revised extensively to accomodate all physical cases of the Hulburt—Hirschfelder potential, and the required numerical methods are described and justified. The revised program substantially extends the range of potentials for which collision integrals can be calculated.

I. INTRODUCTION

Expressions for transport properties of dilute gases are provided by the well-known solution of the Boltzmann equation due to Chapman and Enskog.[1] The transport properties are functions of collision integrals,[1] which are integrals over all classical binary collisions with a weight factor which depends on the angle of scattering. Although the formal expressions for the collision integrals are simple, difficulties are often encountered in their numerical evaluation. In particular, for realistic potentials with an attractive well, orbiting can occur[1,2]; i.e., for certain energies and impact parameters the scattering angle becomes negatively infinite, and the integrand, though bounded, undergoes oscillations of infinite frequency.

Several computer programs have been developed to calculate collision integrals, the most widely used being that of O'Hara and Smith.[3,4] Extensive tables of collision integrals generated from that program have been published.[5] The standard procedure for correlation of dilute gas transport properties data involves choosing a potential with adjustable parameters, e.g., the m-6-8 potential,[6] and varying the parameters to optimize agreement between calculated and measured properties. With such a procedure, dilute gas transport properties and the second virial coefficient of gases may be correlated simultaneously to high precision.[6]

In the most general case, a potential such as the m-6-8 is not even qualitatively appropriate, since for some interatomic states the potential can have both a long-range maximum and a second minimum. An example of a "general purpose" potential which can accommodate such features is the Hulburt–Hirschfelder (HH) potential,[7] whose parameters are not adjustable and are determined entirely from spectroscopic data. Not only is use of this potential more satisfying in principle than the use of potentials with adjustable parameters, but also it is essential when trying to predict transport properties in situations outside the range accessible to laboratory measurement. Such predictions are of practical interest, for example, the prediction of transport properties of the layer of monatomic carbon gas outside the carbonaceous ablation heat shield of a space capsule during entry into a planetary atmosphere.[8]

In general, the existing O'Hara–Smith program[4] is not suitable for the calculation of collision integrals with the HH potential. The program is designed for potentials which are infinite when the interatomic distance $r=0$ and which have a positive repulsive core, a single negative minimum, and attractive tail; purely repulsive potentials are also allowed. The HH potential is finite at $r=0$, which fact requires a minor revision of the program discussed in Appendix A, but the multiple ex-

[a)] Contribution of the National Bureau of Standards, not subject to copyright.

[b)] The use of a specific tradename is necessary in order to specify precisely the speed and efficiency of a computer program. Use of the tradename in no way implies approval, endorsement, or recommendation by the National Bureau of Standards.

[c)] Permanent address: The Procter and Gamble Company, Miami Valley Laboratories, P. O. Box 39175, Cincinnati, OH 45247.

 0021-9606/82/130434-14$02.10 © 1982 American Institute of Physics

trema require much more substantial revisions. Surprisingly, even for some single-minimum HH potentials the double-minimum feature, in embryonic form, qualitatively changes the binary collision dynamics and thereby causes the O'Hara–Smith program to fail. It turns out, as we shall show, that there are five physically separate cases of the HH potential, and problems of physical interest embrace all five possibilities.

Elsewhere, we have predicted the transport properties of particular dilute gases with the HH potential for situations both within[9] and outside[10] the range of laboratory measurement. Central to this work has been the development of a revised collision integral program, valid for all cases of the HH potential.

The objective of this paper is twofold: to analyze and classify the different types of HH potentials and their associated binary collisions, and to describe the numerical techniques employed in the generalized collision integral program. It is emphasized that our numerical methods apply to a general class of potentials, of which the HH family is but one example. Since we wish to emphasize the physics, computational details, wherever possible, are relegated to the appendices. However, we stress that an understanding of binary collision dynamics of the HH potential is an essential prerequisite to construction of a successful numerical integration program.

We begin in Sec. II with a definition and description of the Hulburt–Hirschfelder potential, including qualitative changes that occur due to variation of its parameters. In Sec. III we review the usual treatment of orbiting collisions for "standard" or "type 1" potentials and indicate where that treatment breaks down. Section IV provides a brief description of the O'Hara–Smith collision integral program (more detail is provided in the appendices). The binary collision dynamics of potentials of type 2 through 5 are deduced in Secs. V through VIII, respectively. A summary of results and evaluation of the performance of the revised computer program is given in Sec. IX. The appendices are primarily concerned with technical points, mostly presented in tabular form.

The following paper[10] presents a particular application of the present techniques; namely, the transport properties of high temperature monatomic carbon gas.

II. THE HULBURT–HIRSCHFELDER POTENTIAL

It is customary in numerical calculations to express potential energy functions in terms of reduced, dimensionless units. For realistic potentials, i.e., those with a repulsive core and at least one attractive well, the standard convention is to define reducing variables ϵ and σ, where

$$\min[\phi(r)] = -\epsilon \tag{1}$$

and σ is the smallest root of

$$\phi(\sigma) = 0 \ . \tag{2}$$

The reduced distance r^* and potential ϕ^* are then defined by

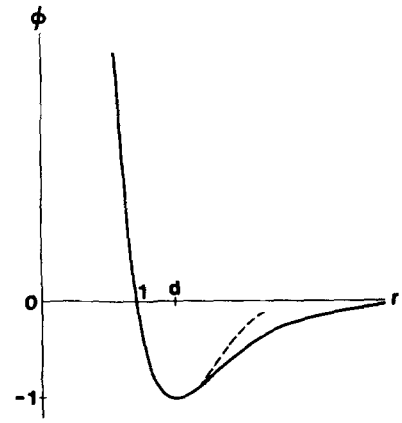

FIG. 1. Morse potential (solid line) and Hulburt–Hirschfelder potential for $\beta > 0$, $\gamma > 0$ (dashed line).

$$r^* = r/\sigma \ , \tag{3}$$

$$\phi^* = \phi/\epsilon \ . \tag{4}$$

The Hulburt–Hirschfelder(HH) potential,[7] expressed in reduced form, is

$$\phi^*(r^*) = \exp[-2a(r^*/d-1)] - 2\exp[-a(r^*/d-1)] + \beta(r^*/d-1)^3[1+\gamma(r^*/d-1)]\exp[-2a(r^*/d-1)] \ , \tag{5}$$

where a, β, and γ are parameters of the potential determined from spectroscopic data (the precise recipe is described elsewhere[10]) and d is the ratio of r_e, the position of the primary minimum in the potential, to σ. With the constraint of Eq. (2), d is not a free parameter but, rather, depends on a, β, and γ and is determined numerically as a function of those parameters. For convenience, we henceforth use reduced units exclusively in this paper and drop the asterisks on ϕ^* and r^*.

The first two terms of Eq. (5) yield a form of the well-known Morse potential.[11] Thus, the Morse potential is the special case, $\beta = 0$, of the HH potential. The Morse potential is plotted in Fig. 1 as the solid line.

The third term of Eq. (5) vanishes at the bottom of the potential well. For positive β and γ, the third term is positive for $r > d$. The full HH potential is shown schematically by the dotted line of Fig. 1.

It is seen from Eq. (5) and the figure that, for sufficiently large β and/or γ, the potential can have a maximum for some $r > d$. Thus, the HH potential can accommodate the long-range maxima known to exist for some systems.[12]

However, since the second term of Eq. (5) undergoes the slowest decay with increasing r, $\phi(r)$ will be negative for sufficiently large r in *all* cases. Thus, those potentials which have a maximum must also have, at a larger distance, a second minimum. This is consistent with the physical idea that, at sufficiently large separations, all molecules should attract one another.[13]

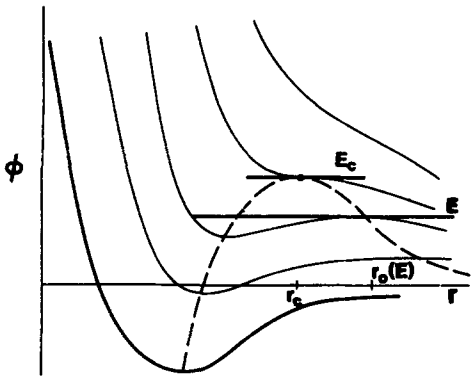

FIG. 2. Schematic plot of effective potential curves and locus of their extrema (dashed line) for a type 1 potential (bold line).

III. ORBITING COLLISIONS: STANDARD (TYPE 1) POTENTIALS

The Chapman–Enskog theory[1] predicts dilute gas transport properties to be functions of the reduced collision integrals

$$\Omega^{(l,s)*} = C_{ls} \int_0^\infty E^{s+1} e^{-E/kT}\, dE \int_0^\infty b\, db (1 - \cos^l \chi) \ , \qquad (6)$$

where C_{ls} is a constant[1] (not important for our present interests), k is Boltzmann's constant, T is the temperature, and χ is the scattering angle for a binary collision with relative total energy E and impact parameter b,

$$\chi = \pi - 2b \int_{r_m}^\infty \frac{dr}{r^2 \left[1 - \frac{b^2}{r^2} - \frac{\phi(r)}{E}\right]^{1/2}} \ , \qquad (7)$$

and r_m, the minimum relative distance or turning point, is the largest value of r such that the expression in brackets in the denominator is zero.

For potentials for which χ is a smooth function of E and b, e.g., purely repulsive potentials,[14] the calculation reduces to a simple, straightforward numerical integration problem. On the other hand, for potentials with attractive wells, χ has singularities as a function of E and b because of a phenomenon known as *orbiting*,[2] which is best described by means of Fig. 2.

For a given E and b, we define the "effective potential," including a centrifugal barrier term, to be

$$\phi_{eff}(r) = \phi(r) + Eb^2/r^2 \ . \qquad (8)$$

A given potential curve determines a family of effective potential curves, as shown in Fig. 2, where each curve depends on E and b only through the combination (Eb^2). We emphasize that Fig. 2, as well as similar subsequent figures, are purely schematic and are distorted to highlight essential qualitative physical features. In particular, the points of greatest curvature are usually much sharper than indicated in the figures. Also, in later figures with long-range extrema, the sizes of these extrema relative to the primary well are generally exaggerated.

The integrand of Eq. (7) is proportional to $[E - \phi_{eff}(r)]^{-1/2}$, i.e., the inverse square root of the vertical distance, in Fig. 2, between the effective potential curve and the horizontal line of constant E. For this energy, a single value of b exists such that the associated effective potential curve is *tangent* to the line of constant E as shown, in which case the integrand of Eq. (7) has a nonintegrable infinity. (The integrand always has a singularity at $r = r_m$, but in general this is an integrable, inverse-square-root singularity.) For this particular value of b, χ is negatively infinite, i.e., orbiting takes place. Specifically, the two particles orbit around each other for an infinite time at a relative distance defined as $r_0(E)$, where the point of tangency occurs.

For small values of (Eb^2), the effective potential curves have minima and maxima as shown. As (Eb^2) increases, the effective potential curve eventually has a point of inflection of zero slope at the point (E_c, r_c), by definition the critical energy and distance. The effective potential curves are monotonically decreasing for larger values of (Eb^2).

With a "standard" or type 1 potential, orbiting does not occur for $E > E_c$, and for each energy $E < E_c$ there exists a unique orbiting impact parameter $b_0(E)$. The scattering angle χ as a function of b is shown qualitatively in Figs. 3(a) and 3(b).

To determine $b_0(E)$, we first identify the value of r, for a fixed E, at which $\phi_{eff}(r)$ can have an extremum. It is easily shown that the required condition is

$$E = z(r) \ , \qquad (9)$$

where

$$z(r) = \phi(r) + \tfrac{1}{2} r\phi'(r) \qquad (10)$$

and a prime denotes differentiation with respect to r.

The function $z(r)$ is plotted as the dashed line in Fig. 2. Note from the above discussion that

$$\max[z(r)] = E_c \ . \qquad (11)$$

The extremum is a maximum if

$$z'(r) = \tfrac{3}{2}\phi'(r) + \tfrac{1}{2} r\phi''(r) < 0 \qquad (12)$$

and is a minimum if

$$z'(r) > 0 \ . \qquad (13)$$

For $E < E_c$, Eq. (9) has two roots, one, $r_0 > r_c$, giving a maximum in the effective potential curve and the other, $r_1 < r_c$, giving a (physically unimportant) minimum in a different effective potential curve. The former root $r_0(E)$ defines the radius at which orbiting occurs; the critical impact parameter is then given by

$$b_0(E) = r_0[1 - \phi(r_0)/E]^{1/2} \ . \qquad (14)$$

While the above description of orbiting is mostly well known, what is usually overlooked are the precise conditions under which such a description is valid. In particular, it does not suffice that, for r greater than d, the potential rise monotonically to zero as $r \to \infty$. Rather, the proper condition is that $z(r)$ rise monotonically to a maximum value E_c at r_c and, for $r > r_c$,

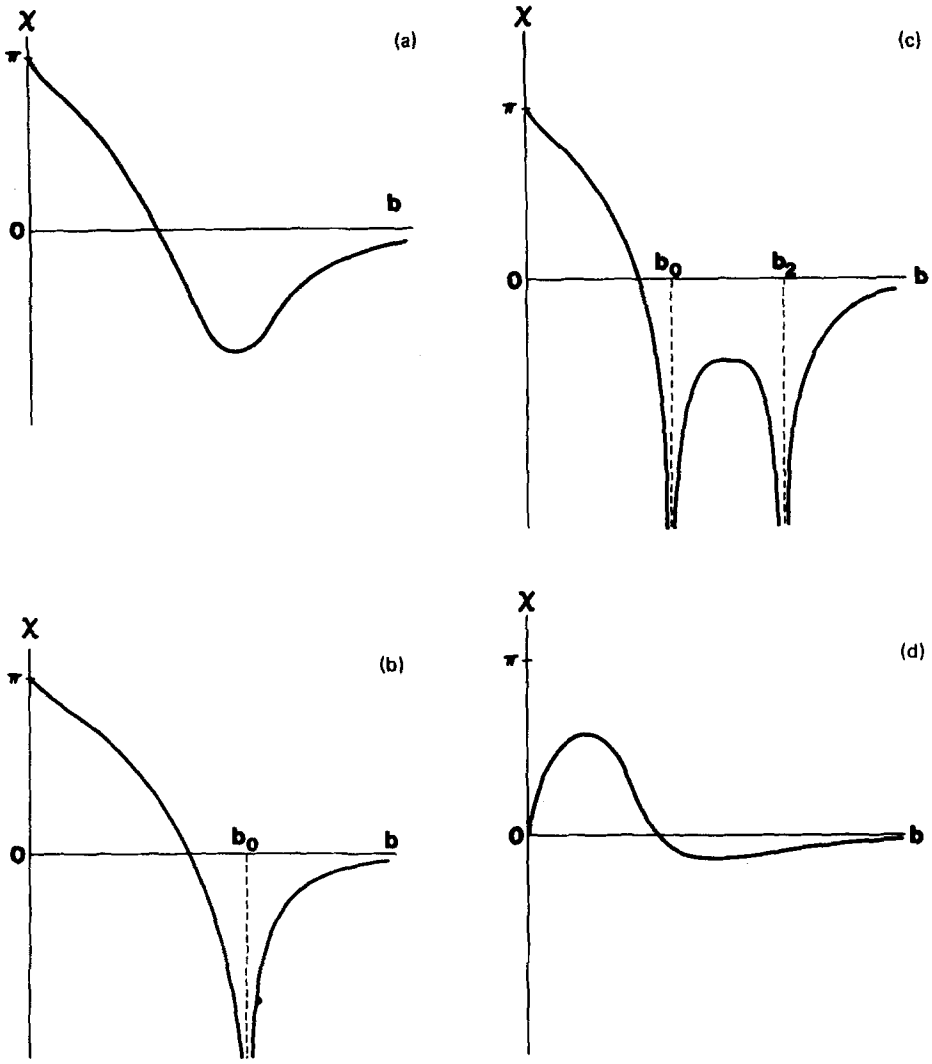

FIG. 3. Scattering angle χ as a function of impact parameter b (schematic). (a) The curve for χ starts at π, decreases to a negative minimum and approaches zero from below for large b ($E > E_c$). (b) For orbiting conditions, $E < E_c$, χ becomes negatively infinite as $b \to b_0$. (c) For double orbiting, χ becomes negatively infinite at two places, b_0 and b_2. (d) If $E > \phi(0)$, then $\chi = 0$ if $b = 0$ and χ has a positive maximum.

decrease monotonically to zero as $r \to \infty$. As we demonstrate in Sec. V, the former condition does not imply the latter. In our terminology, potentials which obey the latter condition are type 1 potentials. The HH potential is type 1 for sufficiently small β or γ. A particular example is the potential for sodium vapor; the HH parameters are

$$a = 2.6361 \; ; \quad \beta = 4.6428 \; ; \quad \gamma = 1.7720 \; . \tag{15}$$

IV. THE O'HARA–SMITH PROGRAM

An efficient computer program to integrate numerically Eq. (6) for a type 1 potential has been developed by O'Hara and Smith.[3] The starting point for our numerical work has been the NBS version of the O'Hara–Smith program,[15] coded by J. F. Ely, and differs somewhat from the final published version of O'Hara and Smith.[4]

Numerical quadratures have the general form

$$\int_a^b f(x)\,dx \approx \sum_{i=0}^{N} w_i f(x_i) \; , \tag{16}$$

where the x_i are abscissas, $a \le x_i \le b$ and the w_i are weight factors. The most efficient quadratures are those that approximate the actual integral, to within some specified accuracy, with N as small as possible.

O'Hara and Smith employ the Clenshaw–Curtis quadrature formula,[16] which has the following advantages[3]:

(1) The abscissas on the fundamental interval $[-1, 1]$ are simple trigonometric functions, i.e.,

$$x_n = \cos \frac{n\pi}{N} \tag{17}$$

for N subintervals, $n = 0, \ldots, N$, in contrast to, for example, Gauss–Legendre quadratures for which the abscissas are roots of a Legendre polynomial. (2) Abscissas for a quadrature with N subintervals are included among those for $2N$ subintervals, again unlike Gaussian quadrature. (3) The Clenshaw–Curtis formalism includes an error estimation technique,[3] involving a sum of the same form as Eq. (16), which is very reliable so long as the integrand is smooth and not peaked in the center of the interval (where the abscissa density is lowest). (4) A particularly convenient variable transformation may be used to handle integrands with a singularity (inverse-square-root or less) at one end [Eq. (23)].

Features (2) and, particularly, (3) make possible a very efficient procedure for numerical integration. By successively doubling the number of subintervals, the

program uses the optimal number of functional evaluations for a given input accuracy requirement. This procedure provides flexibility for users with different accuracy requirements and the opportunity for quick, inexpensive feasibility studies prior to lengthy, more accurate calculations.

The technique is particularly useful for Chapman–Enskog collision integrals. As explained in Sec. III, their integrands are simply behaved over certain regions of the volume of integration and highly oscillatory over other regions. The O'Hara–Smith program *automatically* uses fewer points for the simply behaved regions and more points for the oscillatory regions, as required.

For finite intervals of integration, a simple linear transformation suffices to determine the required abscissas. To evaluate

$$\int_0^\alpha f(y)\,dy$$

with Eqs. (16) and (17), the transformation

$$y = \tfrac{1}{2}\,\alpha(x+1) \tag{18}$$

leads to the expression

$$\int_0^\alpha f(y)\,dy = \frac{\alpha}{2}\sum_{n=0}^{N} w_n f(y_n)\ , \tag{19}$$

where $y_n = y(x_n)$.

In the O'Hara–Smith program, normally an integral on $[0,\infty]$ is evaluated by splitting the interval at approximately the maximum of the integrand and by inversion of the upper part, i.e.,

$$\int_0^\infty f(y)\,dy = \int_0^\alpha f(y)\,dy + \int_0^{1/\alpha} f\left(\frac{1}{z}\right)dz/z^2 \tag{20}$$

and integrals from a finite limit to infinity are performed with a similar inversion.

An alternate transformation designed for singular integrands is

$$y = \alpha\cos\left[\frac{\pi}{4}(1+x)\right]\ , \tag{21}$$

which yields the quadrature formula

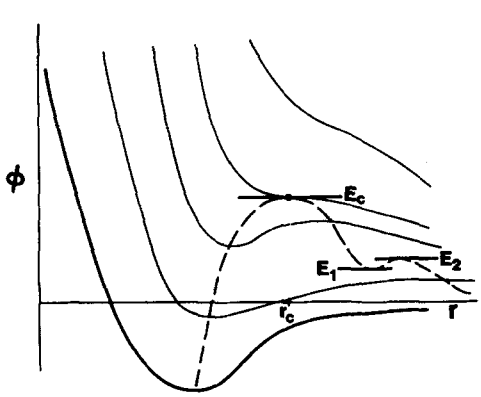

FIG. 4. Schematic plot of effective potential curves and locus of their extrema (dashed line) for a type 2 potential (bold line).

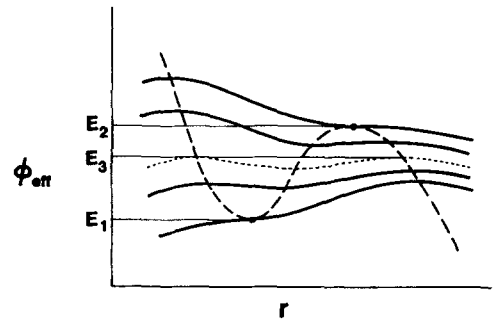

FIG. 5. Magnified view of the region near the kink of $z(r)$ in Fig. 4.

$$\int_0^\alpha f(y)\,dy = \frac{\pi}{4}\sum_{n=0}^{N} w_n\, y_{N-n} f(y_n)\ , \tag{22}$$

where $y_n = y(x_n)$ according to Eqs. (17) and (21). The abscissas thus conveniently play a dual role as weight factors for the transformation.

When $f(y)$ has a singularity at $y=\alpha$, which is inverse-square-root or less, Eq. (22) becomes

$$\int_0^\alpha f(y)\,dy = \frac{\pi}{4}\left\{\sum_{n=0}^{N-1} w_n\, y_{N-n} f(y_n) + w_N \lim_{y\to\alpha}\left[\sqrt{\alpha^2-y^2}\,f(y)\right]\right\}\ . \tag{23}$$

O'Hara and Smith use this transformation for several different purposes: (a) to supress an actual inverse-square-root singularity, for example, the singularity at $r=r_m$ of Eq. (7); (b) to suppress the infinite oscillations in the b integrand of Eq. (6) at orbiting, after the b integral is split at $b=b_c(E)$ as in Eq. (20); (c) to suppress large but finite oscillations in the same b integrand for E slightly larger than E_c, where $|\min(\chi)|$ can be several multiples of π [cf. Fig. 3(a)], or (d) to perform more efficiently an integral with a large but finite peak in the integrand at or near one end.

The essential strategy of the O'Hara–Smith collision integral program is first to characterize qualitatively the different possibilities for binary collisions, then to identify thereby the singularities and near-singularities in Eqs. (6) and (7), then to split the integrals, where necessary, at such singular points and finally to use the transformation of Eqs. (21) and (23) to suppress such singular behavior. In this work we follow, as closely as possible, such a strategy in order to generalize the O'Hara–Smith program for potentials with more complicated binary collision dynamics.

V. TYPE 2 POTENTIALS

Figures 4 and 5 display the family of effective potential curves for "type 2" potentials. As seen from Fig. 4, a type 2 potential is similar to type 1 in that $\phi(r)$ increases monotonically to zero as r increases from d to infinity. However, the function $z(r)$, the locus of extrema of the effective potential curves, does not decrease monotonically for $r > r_c$. Rather, it has a minimum and a second maximum as shown. An example is the HH potential for cesium vapor, where

$$a = 3.2935\ ,\quad \beta = 12.463\ ,\quad \gamma = 2.3263\ . \tag{24}$$

The boundary in parameter (a,β,γ) space between type 1 and 2 potentials is the boundary between the regions where the equation

$$z'(r) = \tfrac{3}{2}\,\phi'(r) + \tfrac{1}{2}\,r\phi''(r) = 0 \tag{25}$$

has, respectively, one or three finite roots.

Figure 5 shows a closeup of the region near the "kink" in the function $z(r)$ and the associated family of effective potential curves. The minimum occurs at $z(r) = E_1$, the maximum at $z(r) = E_2$.

The lowest effective potential curve shown has a point of inflection with zero slope at $E = E_1$ and a single maximum to the right. All effective potential curves below this one have single maxima. The uppermost curve has, similarly, a point of inflection with zero slope at $E = E_2$ and a single maximum to the left; all effective potential curves above this one have single maxima also.

Effective potential curves between these two, however, have *two* maxima. There exists a particular effective potential curve, shown by the dotted line, for which the two maxima occur at equal energies $E = E_3$. The most complicated binary collisions for the HH potential occur at this energy and impact parameter (approached from above), in which case the particles, during a single collision, orbit each other twice at two separate radii.

For effective potential curves below the dotted one, the inner maximum (smaller r) is at a lower energy than the outer maximum. For curves above the dotted one, the converse is true. In the former case, the inner maxima do not lead to orbiting, since particles which might orbit at that radius would not be able to penetrate the outer centrifugal barrier. In the latter case, however, both maxima can lead to orbiting.

It is seen from these considerations that a single critical impact parameter exists for energies such that $E < E_3$ and $E_1 < E < E_c$. However, for all energies $E_3 < E < E_1$, there are *two* critical impact parameters corresponding to inner and outer maxima of the appropriate effective potential curves. As expected on intuitive grounds, the larger of the two impact parameters is associated with the larger orbiting radius. The scattering angle as a function of impact parameter is shown for such cases in Fig. 3(c).

Necessary modifications of the O'Hara–Smith program to determine the critical impact parameters, scattering angles, and collision integrals are described in the appendices.

VI. TYPE 3 POTENTIALS

When β or γ becomes sufficiently large, the potential will develop new extrema as shown in Fig. 6. We classify this case as a "type 3" potential. The potential has, in addition to the primary well, a negative maximum and, beyond that, a small negative minimum. An example is the HH potential for potassium, where

$$a = 2.9825\ ,\quad \beta = 10.6439\ ,\quad \gamma = 2.1828\ . \tag{26}$$

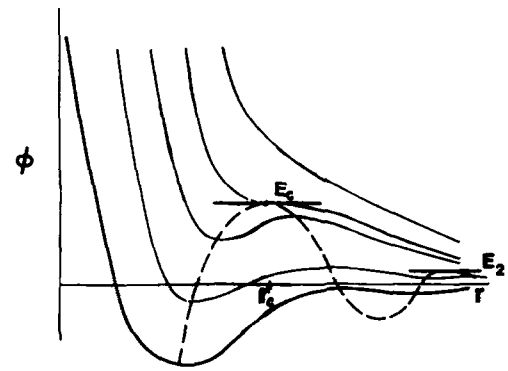

FIG. 6. Schematic plot of effective potential curves and locus of their extrema (dashed line) for a type 3 potential (bold line).

The boundary in parameter space between type 2 and 3 potentials is the boundary between the regions where the equation

$$\phi'(r) = 0 \tag{27}$$

has, respectively, one or three finite roots.

As shown in the figure [cf. Eq. (10)] the curve for $z(r)$ crosses the potential curve at the maximum and minimum of the latter. Energies E_1, E_2, and E_3 may be defined similarly to those of the previous section; however, here E_1 is negative and not physically relevant.

The binary collision dynamics closely parallel that of type 2 potentials. For $E < E_3$ and $E_2 < E < E_c$ there is a single critical impact parameter, whereas for $E_3 < E < E_2$ there are two separate critical impact parameters. Modifications of the program for such potentials are described in the appendices.

In practice, a type 2 potential such that $E_1 < E_{min}$, where E_{min} is the minimum energy needed for the quadrature of Eq. (6) [see Appendix F], need not be distinguished from a type 3 potential. In such cases, since it is unnecessary for collision integral evaluation, the program on occasion does not make a detailed search to check the potential type and prints a statement that the type is ambiguous.

VII. TYPE 4 POTENTIALS

As β or γ is further increased, the maximum in the potential can change from a negative to a positive value. The energy of the positive maximum is defined to be E_L (at $r = r_L$). Such potentials are classified as type 4 or 5, according as E_L is small or large. The boundary in parameter space between type 3 and 4 potentials is the boundary between the regions where the equation

$$\phi(r) = 0 \tag{28}$$

has, respectively, one or three finite roots.

As before, E_2 is defined to be the energy of the second maximum in the function $z(r)$. For positive E_L, type 4 potentials by definition have the property that

$$E_L < E_2\ , \tag{29}$$

whereas, for type 5 potentials,

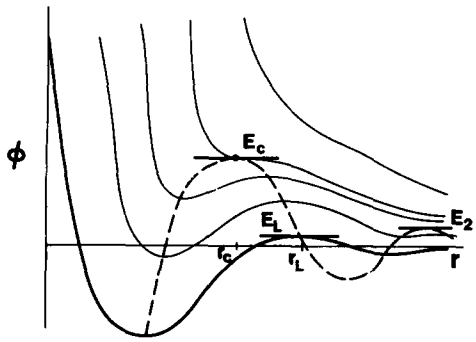

FIG. 7. Schematic plot of effective potential curves and locus of their extrema (dashed line) for a type 4 potential (bold line).

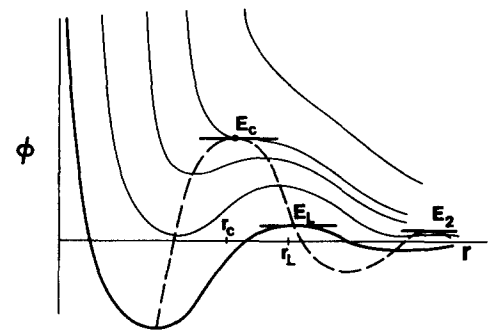

FIG. 8. Schematic plot of effective potential curves and locus of their extrema (dashed line) for a type 5 potential (bold line).

$$E_L > E_2 \ . \tag{30}$$

An example of a type 4 potential is the HH potential for the $^3\Delta_u$ state of carbon, where

$$a = 4.0971 \ , \quad \beta = 24.1056 \ , \quad \gamma = 4.0672 \ . \tag{31}$$

The effective potential curves for type 4 potentials are shown in Fig. 7. There exists a particular effective potential curve (not shown) which has a point of inflection, with zero slope, at $E = E_2$ and a single maximum to the left. All effective potential curves below this one have two maxima, with the inner one occurring at a larger energy than the outer one.

Therefore, for $E < E_L$ and $E_2 < E < E_c$ each energy has a single critical impact parameter. For $E_L < E < E_2$, there are two critical impact parameters. Unlike types 2 and 3, there is no energy for which the values of the two critical impact parameters are equal. The lower critical b approaches zero as $E \to E_L$ from above. Again, details of required changes in the program are described in the appendices.

VIII. TYPE 5 POTENTIALS

When Eq. (30) holds, the potential is classified as type 5. Effective potential curves for this case are shown in Fig. 8. An example is the HH potential for the $^1\Pi_g$ state of carbon, where

$$a = 5.2665 \ , \quad \beta = 68.2301 \ , \quad \gamma = 5.4861 \ . \tag{32}$$

The energy E_2 may be interpreted here as a second critical energy. For $E < E_2$ and $E_L < E < E_c$, there is a single critical impact parameter. However, in contrast to previous cases, for $E_2 < E < E_L$ orbiting is *not* possible. All such collisions have a distance r_m of closest approach greater than r_L, and above such distances, for that energy range, there are no maxima in the effective potential curves.

The binary collision dynamics for this type are significantly simpler than that of the three previous types, since no "double orbiting" occurs. There are two distinct intervals of possible orbiting radii corresponding, respectively, to the two potential wells. Again, required program changes are described in the appendices.

It should be mentioned that there exist model potentials, not within the HH family, which have a positive maximum at $E = E_L$ and, as r increases to infinity, approach zero from *above* without a second minimum. Such potentials, for example, are used to represent the dipole–dipole interaction of nonspherical molecules.[15] For such potentials, orbiting does not occur for $E < E_L$ and there is a single critical impact parameter for energies such that $E_L < E < E_c$. The unmodified O'Hara–Smith program is already equipped to handle such potentials, and within our classification scheme these are special cases of type 1 potentials.

It is instructive to plot the boundaries between potential types in parameter $(a - \beta - \gamma)$ space. Although this in principle requires a three-dimensional plot, it is possible to devise an illuminating two-dimensional plot as follows. If we define

$$y = a(r/d - 1) \ , \tag{33}$$

then Eq. (5) for the HH potential is

$$\phi(r) = e^{-2y} - 2e^{-y} + \frac{\beta}{a^3} y^3 \left(1 + \frac{\gamma}{a} y\right) e^{-y} \ . \tag{34}$$

The 2–3 and 3–4 boundaries, according to Eqs. (27) and (28), depend only on ϕ and its derivative, and thus depend on the HH parameters only through the combinations (β/a^3) and (γ/a). On a two-dimensional plot with these combinations as the axes, Fig. 9, the 2–3 and 3–4 boundaries are single lines, independent of a.

The 1–2 and 4–5 boundaries, according to Eqs. (25),

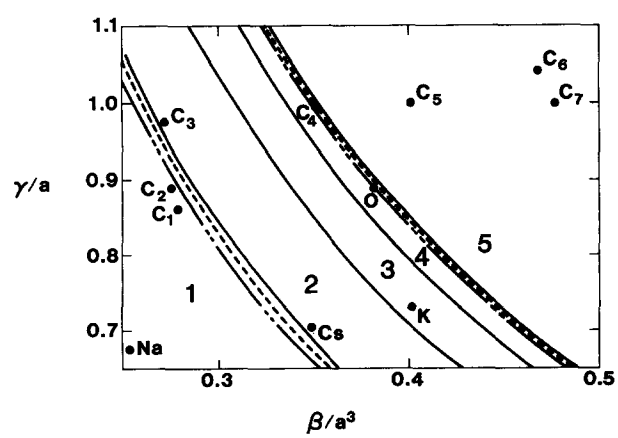

FIG. 9. Type boundaries in the space of HH potential parameters; $a = 2$ is broken line, $a = 3$ is dashed line, and $a = 4$ is solid line. Specific potentials are identified in Table I.

TABLE I. HH potentials displayed in Fig. 9.

Symbol	Molecular state	a	β	γ
Na	Sodium $^1\Sigma_g^+$	2.6361	4.6428	1.7720
K	Potassium $^1\Sigma_g^+$	2.9825	10.6439	2.1828
Cs	Cesium $^1\Sigma_g^+$	3.2935	12.4630	2.3263
O	Oxygen $^3\Sigma_u^+$	5.2910	56.4574	4.7152
C_1	Carbon $^5\Pi_g$	3.6002	13.0005	3.0991
C_2	Carbon $^1\Sigma_{g2}^+$	3.4481	11.2288	3.0636
C_3	Carbon $^3\Sigma_u^+$	3.6798	13.4984	3.5801
C_4	Carbon $^3\Delta_u$	4.0971	24.1056	4.0672
C_5	Carbon $^5\Sigma_g^+$	4.3308	32.4911	4.3260
C_6	Carbon $^1\Sigma_u^-$	4.5978	46.2266	4.6065
C_7	Carbon $^1\Pi_g$	5.2665	68.2301	5.4861

(29), and (30), depend on $z(r)$, hence r, as well as ϕ. Thus, in addition to their dependence on (β/a^3) and (γ/a), these boundaries also depend on a, but weakly so. Figure 9 shows the 1–2 and 4–5 boundaries, computed numerically with the scanning subroutine from our program, for $a = 2$, 3, and 4. Also shown are the positions on the graph of various HH potentials for some systems of practical interest, whose properties are listed in Table I.

IX. SUMMARY AND CONCLUSIONS

By a generalization of the O'Hara–Smith numerical integration program,[3,4] we have developed a successful technique for evaluation of gaseous transport collision integrals for the Hulburt–Hirschfelder potential,[7] a monatomic potential which is determined from spectroscopic data, has no adjustable parameters, and can accommodate the long-range maxima and second minima found in certain systems.[12] The development requires a detailed study of the qualitative dynamics of binary collisions. We have classified the HH potential into five types, each with a distinct pattern of binary collision dynamics. In modifying and following the philosophy of the O'Hara–Smith program, we identify singularities and near-singularities of the integrands, split the intervals of integration at the singular points, and evaluate the integrals with a Clenshaw–Curtis quadrature[16] and a variable transformation to suppress singular behavior where necessary.

In assessing the reliability of our numerical output, we follow Klein, *et al.*,[5] and make a distinction between *accuracy*, the consistency of our values with previous and independent numerical studies, and *precision*, reflected here in the ability of our numerical values to pass certain self-consistency checks. As for accuracy, the only previous calculations of transport collision integrals for the HH potential family to our knowledge have been for the Morse potential. We have compared our values for the Morse potential with those of Smith and Munn,[2] who used a precursor of the O'Hara–Smith program based on Gaussian quadratures. The agreement is always within a few parts in 10^3.

We checked the precision of our results by adding a loop to the program which imposed successive accuracy inputs of 10^{-2}, 10^{-3}, 10^{-4}, and 10^{-5}. The loop also calculated, on each cycle, the relative error between the two most recent runs, and these were compared with the maximum allowable error. For example, if the error estimation technique is reliable, the maximum allowable relative error between the runs with accuracy input of 10^{-2} and 10^{-3} is 0.011.

The results are shown in Table II. Sample HH potentials of each of the five types were chosen. All $\Omega^{(l,s)*}$ integrals for $1 \le l \le s$, $l \le s \le 3$ were evaluated for 46 reduced temperatures $T^* = kT/\epsilon$ ranging from a low of $T^* = 0.004$ to a high of $T^* = 200$. The lowest temperature, much lower than normally used in practice, provides a severe test of the methods developed to take care of double orbiting. The notation $n_1/n_2/n_3$ indicates that (out of 276 possibilities) n_1 results were between one and two times the maximum allowable relative error, n_2 results were between two and three times that error, and n_3 results were more than three times that error. For the sake of comparison, we have included results of the same test on the *unmodified* O'Hara–Smith program with a Lennard-Jones 12-6 potential.

The results are excellent for the 10^{-2}–10^{-3} and 10^{-3}–10^{-4} comparisons. Only for a very small number of cases (mostly at very low T^*) is the maximum allowable error exceeded, and in none of these is it exceeded drastically. However, the 10^{-4}–10^{-5} comparison leads to a large number of excessive relative errors. As currently constructed, the program allows for a maximum of 64 Clenshaw–Curtis subintervals [$N = 65$ in Eq. (16)] and prints out warning messages if convergence has not been achieved at 64 intervals. No such warming messages were printed through the accuracy input of 10^{-4}, but a multitude of them were printed at 10^{-5}. We conclude that accuracy inputs of 10^{-5}, ordinarily never needed in practice, require (at least) an increase to 128 of the maximum number of Clenshaw–Curtis intervals available.

The most important conclusion is that the precision of the modified program for all types of HH potential compares most favorably with that of the unmodified program and the Lennard-Jones 12-6 potential, which has considerably simpler binary collision dynamics. It should be mentioned that the majority of collision integral comparisons were an order of magnitude or more *better* than the greatest allowable error. This is because doubling the number of Clenshaw–Curtis subinter-

TABLE II. Precision analysis of program. The number of collision integrals, grouped into intervals, which violate the accuracy requirements are listed.

Potential	$10^{-2}/10^{-3}$	$10^{-3}/10^{-4}$	$10^{-4}/10^{-5}$
Type 1	4/0/0	5/0/0	12/14/3
Type 2	1/1/0	1/0/0	29/26/0
Type 3	0/0/0	3/0/0	18/18/2
Type 4	0/0/0	0/0/0	failure
Type 5	0/0/0	0/0/0	74/15/0
Lennard-Jones	0/0/0	2/0/0	25/2/3

vals ordinarily decreases the error by two to three orders of magnitude. The error estimation technique is conservative and is intended to give (almost) a *guarantee* of the desired accuracy; the "expectation value" of the error is generally much smaller.

The running time of the program is generally larger for the middle potential types, but the program is quite efficient for all cases. As examples, on a CDC 6400 computer, a run of a type 1 potential with 46 temperatures and $l \leq s$, $s \leq 3$ took 34.3 s at 10^{-2} accuracy and 179.7 s at 10^{-4} accuracy, a run of a type 3 potential took 56.2 and 363.2 s, respectively, and a run of a type 5 potential took 35.0 and 170.4 s, respectively. By comparison, equivalent runs of the Lennard-Jones 12-6 potential with the unmodified program took 26.3 and 91.4 s, respectively.

Finally, we note that, although our computer program has been designed with the Hulburt–Hirschfelder potential in mind, it is suitable for any other potential with an equivalent qualitative pattern of binary collisions. One of us (J. C.R.), together with co-workers at the National Bureau of Standards, is preparing an NBS Technical Note[17] which will include a complete listing of the revised program and a set of interchangeable potential subroutines for various different interparticle potentials, including the HH and m-6-8 families.

ACKNOWLEDGMENTS

The authors thank D. J. Evans, S. Haber, J. F. Ely, and H. J. M. Hanley for valuable suggestions. This work was supported in part by NASA grant NASA NSG 1369. One of the authors (L.B.) would like to acknowledge a Visiting Fellowship at the Cooperative Institute for Research in Environmental Sciences.

APPENDIX A: CHANGES FOR FINITE POTENTIAL AT THE ORIGIN

For a potential which is infinite at $r=0$, e.g., the Lennard-Jones 12-6, the scattering angle χ equals π for a head-on collision ($b=0$). If the potential is finite at the origin, $\chi(b=0)=\pi$ for collision energies less than $\phi(0)$. However, for energies greater than $\phi(0)$ the particles pass through each other during a head-on collision, and $\chi(b=0)=0$.

The scattering angle as a function of impact parameter is plotted schematically in Fig. 3(d) for $E>\phi(0)$. The angle reaches some maximum value less than π and, thereafter follows qualitatively the pattern of Fig. 3(b). This maximum value of χ decreases with increasing E.

If the potential is infinite at the origin, at very large energies the b integrand of Eq. (6) is peaked approximately at b', defined such that $\chi(b')=\pi/2$. O'Hara and Smith,[3] for this reason, split the b integration interval at b', as in Eq. (20).

However, for the HH potential which is finite at the origin, it is quite likely that the largest energy abscissa required in the integral of Eq. (6) is greater than $\phi(0)$, and, furthermore, that the maximum scattering angle [Fig. 3(d)] is less than $\pi/2$. In this case the program searches numerically for b' in vain and until overflow occurs.

The remedy is simply to bypass, for large energies ($E>10^3 E_c$), the search for b' and to split the b integral, somewhat arbitrarily, at $b=1$. Although this may not be the optimal splitting for all large energies, the exponential factor in Eq. (6) heavily suppresses the integrand at large energies, so that errors in the b integration at such energies have a negligible impact on the overall collision integral.

In all other respects the O'Hara–Smith program works properly for type 1 Hulburt–Hirschfelder or similar potentials.

APPENDIX B: DETERMINATION OF POTENTIAL TYPE AND ORBITING IMPACT PARAMETERS

Before evaluating any integrals, the program scans the potential numerically, $10^{-1}<r<10^4$, to determine its type. Extrema in $\phi(r)$ and $z(r)$ are monitored and the energies E_c, E_2, and E_L are determined to high accuracy. The program aborts if the potential has two maxima (not possible for the HH potential).

Within the orbiting energy regions, arrays of [E, $b_0(E)$, $r_0(E)$] are then constructed. As explained in the text, a single energy can have two orbiting parameters for types 2 and 3 ($E_3<E<E_2$) and type 4 ($E_L<E<E_2$). In such cases we define the inner (smaller) orbiting impact parameter to be $b_0(E)$ and the outer (larger) orbiting impact parameter to be $b_2(E)$ [and, similarly, $r_0(E)$ and $r_2(E)$].

The range of input temperatures and quadrature points determines a unique minimum energy $E_{\min}$ which (except for zero) might be required in the energy integration of Eq. (6). For type 1 potentials an array of orbiting parameters, with approximately 100 elements, is constructed numerically according to the equations

$$E=z[r_0(E)] \text{ (largest root)} , \tag{B1}$$

$$b_0(E)=r_0(E)\{1-[r_0(E)]/E\}^{1/2} , \tag{B2}$$

for $E_{\min}<E<E_c$.

For types 2–5, there are two separate ranges of orbiting parameters, an inner range (smaller values of r_0) and an outer range (larger values of r_0). Two such arrays of orbiting parameters are constructed for these cases. The orbiting impact parameters are $b_{\text{in}}(E)$ for the inner range, and $b_{\text{out}}(E)$ for the outer range. The correspondence with b_0 and b_2 is straightforward, e.g., for type 2, $b_0=b_{\text{out}}$ if $E_{\min}<E<E_3$, $b_0=b_{\text{in}}$, and $b_2=b_{\text{out}}$ if $E_3<E<E_2$, and $b_0=b_{\text{in}}$ if $E_2<E<E_c$. The energy intervals for the various arrays and potential types are listed in Table III.

In subsequent calculations, required values of the orbiting parameters for a given E are found from the arrays by an Aitken interpolation scheme.[18] O'Hara and Smith have found that, if $y=f(x)$ and $x(y)$ must be calculated numerically, it is better, after finding a suffi-

TABLE III. Orbiting parameter arrays.

Potential	Inner array	Outer array
Type 1	$E_{min} < E < E_c$	none
Type 2	$E_1 < E < E_c$	$E_{min} < E < E_2$
Type 3	$E_{min} < E < E_c$	$E_{min} < E < E_2$
Type 4	$E_L < E < E_c$	$E_{min} < E < E_2$
Type 5	$E_L < E < E_c$	$E_{min} < E < E_2$

ciently accurate value $\bar{x}$, to use the self-consistent variables $\bar{y} = f(\bar{x})$ and $\bar{x}$ rather than y and $\bar{x}$ for subsequent numerical integration. We follow this technique for E, r_0, and b_0 wherever possible. However, in a double orbiting region it is not possible to determine algebraically a self-consistent $\bar{E}$, $\bar{b}_0$, and $\bar{b}_2$. This leads to difficulties for very small accuracy inputs, and was responsible for the failure of the type 4 potential with an accuracy input of 10^{-5} in Table II.

For types 2 and 3 the precise calculation of the energy E_3 is unnecessary. From Fig. 6, $b_{in}(E_3) = b_{out}(E_3)$, and it can be seen that, in the range $E_1 < E < E_2$, $b_{in} > b_{out}$ if $E < E_3$, and $b_{in} < b_{out}$ if $E > E_3$. Thus, a given energy in this region is above or below E_3 according to the relative sizes of b_{in} and b_{out}, which are always needed elsewhere in the calculation. This is consistent with the intuitive idea that, for double orbiting, the larger impact parameter must be associated with the larger orbiting radius.

A type 2 potential with $E_1 < E_{min}$ is functionally equivalent to a type 3 potential. In this case, which occurs very infrequently, the scanning routine does not definitively identify the potential type and prints a message that the type identification is ambiguous.

APPENDIX C: DETERMINATION OF THE DISTANCE OF CLOSEST APPROACH

One of the most troublesome aspects of the development of the collision integral program has been the reliable determination of $r_m(b,E)$, the distance of closest approach of a binary collision and the largest root in r of the equation

$$F(r,b,E) = 1 - b^2/r^2 - \phi(r)/E = 0 \ . \qquad \text{(C1)}$$

For nonorbiting energies, Eq. (C1) has one root. But for type 1 potentials, $E < E_c$ and $b > b_c(E)$, Eq. (C1) has three roots, and for the higher potential type it is possible for Eq. (C1) to have as many as *five* roots. Without extreme care, a root-finding technique for r_m will, at some point in the calculation, incorrectly converge on an inner root. The subsequent calculation of the scattering angle, Eq. (7), will cause the program to fail via the attempted calculation of the square root of a negative number.

The algorithm of the O'Hara–Smith program (NBS version) for r_m is as follows: Choose an initial guess r_g for r_m. If $F(r_g) > 0$, repeatedly halve the distance until $F < 0$. Then, or if $F(r_g) < 0$, increase the distance repeatedly until $F > 0$. Converge on the root by bisecting six times. Finally, determine r_m accurately by an Aitken interpolation procedure.[18]

TABLE IV. Choice of r_g.

Potential	Energy	Impact parameter	r_g
Type 1	$E < E_c$	all b	r_0
	$E > E_c$	all b	2.0
Types 2 and 3	$E < E_3$	all b	r_0
	$E_3 < E < E_2$	$b < b_2$	r_0
		$b > b_2$	r_2
	$E_2 < E < E_c$	all b	r_0
	$E > E_c$	all b	2.0
Type 4	$E < E_L$	$b < b_0$	r_L
		$b > b_0$	r_0
	$E_L < E < E_2$	$b < b_2$	r_0
		$b > b_2$	r_2
	$E_2 < E < E_c$	all b	r_0
	$E > E_c$	all b	2.0
Type 5	$E < E_2$	$b < b_0$	r_L
		$b > b_0$	r_0
	$E_2 < E < E_L$	all b	r_L
	$E_L < E < E_c$	all b	r_0
	$E > E_c$	all b	2.0

The original published O'Hara–Smith program[4] includes a feedback mechanism where, if r_m is found to be incorrectly evaluated within the scattering angle subroutine, a corrected r_m is then determined. However, the conditions under which this feedback mechanism is activated are not sufficiently general for all of the potential types we consider. The NBS version of the program does not contain such a feedback mechanism.

After substantial trial and error, we have chosen the following procedure. A feedback mechanism is not included. The above algorithm is used, and convergence onto the proper root is assured by the proper choice of r_g for the given potential type, energy, and impact parameter. The choices of r_g are listed in Table IV.

When multiple roots exist for Eq. (C1), r_g is chosen such that $F(r_g) < 0$ and there is only one root, the desired one, for $r > r_g$, so that the above algorithm converges onto the proper root. These choices can be verified by examination of Figs. 2–8 with the appropriate additional effective potential curves. When only one root of Eq. (C1) exists, we either set r_g equal to one of the orbiting distances for convenience, or we arbitrarily set $r_g = 2.0$.

APPENDIX D: CALCULATION OF THE SCATTERING ANGLE

The scattering angle χ is given by Eq. (7) in terms of an integral which must be calculated numerically. In all cases there are at least two difficulties at the outset, namely the infinite upper limit and the inverse-square-root singularity at $r = r_m$. Following O'Hara and Smith, we take care of the first problem by inversion of the interval [cf. Eq. (20)], and overcome the second problem by use of Eq. (23) which suppresses the singularity at $r = r_m$.

Further difficulties are present for orbiting energies. As described in the following appendix, the integrations over b are split at the orbiting impact parameters and transformations are employed which suppress the singularities at orbiting. Therefore, we insure that the program never attempts the calculation of χ at orbiting, where χ approaches infinity. However, for b slightly less than an orbiting impact parameter, the integrand for χ has a large peak near the orbiting radius, in which case it is more efficient to split the integration interval near the peak than to perform the integration using a single interval, i.e.,

$$\int_0^{1/r_m} dy\,[F(y^{-1},b,E)]^{-1/2} = \int_0^{1/r_0} dy[F(y^{-1},b,E)]^{-1/2} + \int_{1/r_0}^{1/r_m} dy[F(y^{-1},b,e)]^{-1/2}\ , \tag{D1}$$

where $y=r^{-1}$ and F is given by Eq. (C1).

Since the second integrand can have a sharp peak or near-singularity at the lower end as well as the true singularity at the upper end, we require an integration algorithm for the integral

$$\int_\alpha^\beta f(y)\,dy\ ,$$

with singularities (inverse-square-root or less) at both $y=\alpha$ and $y=\beta$. This is accomplished within the O'Hara-Smith program by the dual transformation

$$y=\beta\cos z\ , \tag{D2}$$

$$z=\cos^{-1}\left(\frac{\alpha}{\beta}\right)\cos\left[\frac{\pi}{4}(1+x)\right]\ , \tag{D3}$$

which maps the interval onto $[-1,1]$ in x. The quadrature formula is then

$$\int_\alpha^\beta f(y)\,dy = \frac{\pi}{4}\left[w_0\cos^{-1}\left(\frac{\alpha}{\beta}\right)\lim_{y\to\beta}(\beta^2-y^2)^{1/2}f(y) + \sum_{n=1}^{N-1}\beta w_n z_{N-n}\sin z_n f[y(z_n)] + w_N\left(\cos^{-1}\frac{\alpha}{\beta}\right)^{1/2}\alpha^{-1/2}(\beta^2-\alpha^2)^{1/4}\lim_{y\to\alpha}(y^2-\alpha^2)^{1/2}f(y)\right], \tag{D4}$$

where $z_n=z(x_n)$; see Eq. (17).

The situation is even more complicated in the presence of double orbiting. The integrand for χ can, depending on energy and impact parameter, have a significant peak at $r=r_0$ or $r=r_2$ or, in special cases, at *both* points, in which case it is best to split the interval into three subintervals.

In summary, there are four separate methods for evaluating the scattering angle integral, one of which is optimal for a given potential type, energy, and impact parameter:

(a) Evaluate the integral over the single interval $[0,r_m^{-1}]$ in y by means of Eq. (23). (b) Evaluate the integral over the two subintervals $[0,r_0^{-1}]$ and $[r_0^{-1},r_m^{-1}]$ in y. Use Eq. (23) for the first interval and Eq. (D4) for the second. (c) Utilize method (b) with r_0 replaced by r_2. (d) Evaluate the integral over the three subintervals $[0,r_2^{-1}]$, $[r_2^{-1},r_0^{-1}]$ and $[r_0^{-1},r_m^{-1}]$. Use Eq. (23) for the first interval and Eq. (D4) for the last two.

TABLE V. Calculation of the scattering angle.

Potential	Energy	Impact parameter	Method
Type 1	$E<E_c$	$b<b_0$	(b)
		$b>b_0$	(a)
	$E>E_c$	all b	(a)
Type 2	$E<E_1$	$b<b_0$	(b)
		$b>b_0$	(a)
	$E_1<E<E_3$	$b<b_0$ and	
		$b<b_1(E_1/E)^{1/2}$	(b)
		$b_1(E_1/E)^{1/2}<b<b_0$	(d)
		$b>b_0$	(a)
	$E_3<E<E_2$	$b<b_0$ and	
		$b<b_1(E_1/E)^{1/2}$	(c)
		$b_1(E_1/E)^{1/2}<b<b_0$	(d)
		$b_0<b<b_2$	(c)
		$b>b_2$	(a)
	$E_2<E<E_c$	$b<b_0$	(b)
		$b>b_0$	(a)
	$E>E_c$	all b	(a)
Type 3	$E<E_3$	$b<b_0$	(d)
		$b>b_0$	(a)
	$E_3<E<E_2$	$b<b_0$	(d)
		$b_0<b<b_2$	(c)
		$b>b_2$	(a)
	$E_2<E<E_c$	$b<b_0$	(b)
		$b>b_0$	(a)
	$E>E_c$	all b	(a)
Type 4	$E<E_L$	$b<b_0$	(b)
		$b>b_0$	(a)
	$E_L<E<E_2$	$b<b_0$	(b)
		$b_0<b<b_2$	(c)
		$b>b_2$	(a)
	$E_2<E<E_c$	$b<b_0$	(b)
		$b>b_0$	(a)
	$E>E_c$	all b	(a)
Type 5	$E<E_2$	$b<b_0$	(b)
		$b>b_0$	(a)
	$E_2<E<E_L$	all b	(a)
	$E_L<E<E_c$	$b<b_0$	(b)
		$b>b_0$	(a)
	$E>E_c$	all b	(a)

Following the philosophy of O'Hara and Smith, we split the interval whenever there is a possibility that a sharp peak in the χ integrand can occur. The precise scheme is displayed in Table V. All variables in the table have been defined previously except

$$b_1=b_{1n}(E_1)\ . \tag{D5}$$

Note that, for a type 2 potential, the χ integrand can have two finite maxima only if $Eb^2>E_1b_1^2$.

APPENDIX E: INTEGRATION OVER THE IMPACT PARAMETER

From a numerical integration standpoint, the most challenging aspect of the present problem is the integration over the impact parameter b. The integrand displays a wide range of behavior from very smooth to infinitely oscillatory at orbiting. With double orbiting there are *two* points where the oscillations in the inte-

TABLE VI. Intervals for integration over impact parameter.

Potential	Energy	Division of Intervals
Type 1	$E<E_c$	$(0,b_0)^{(b)},^{(b,d)}$ $[r_0,\infty]$**
Types 2	$E<E_3$	$(0,b_0)^{(b)},^{(b,d)}$ $[r_0,\infty]$**
and 3	$E_3<E<E_2$	$(0,b_0)^{(b)}$, $[r_0,r_{av}]$, $(b_{av},b_2)^{(b)},^{(b,d)}$ $[r_2,\infty]$**
	$E_2<E<2E_2$	$(0,b_0)^{(b)}$, $[r_0,r'_{av}]$, $(b'_{av},b_{2c})^{(c)},^{(c,d)}$ $[r_{2c},\infty]$**
	$2E_2<E<E_c$	$(0,b_0)^{(b)},^{(b,d)}$ $[r_0,\infty]$**
Type 4	$E<E_L$	$(0,b_0)^{(b)},^{(b,d)}$ $[r_0,\infty]$**
	$E_L<E<E_2$	$(0,b_0)^{(b)}$, $[r_0,r_{av}]$, $(b_{av},b_2)^{(b)},^{(b,d)}$ $[r_2,\infty]$**
	$E_2<E<2E_2$	$(0,b_0)^{(b)}$, $[r_0,r'_{av}]$, $(b'_{av},b_{2c})^{(c)},^{(c,d)}$ $[r_{2c},\infty]$**
	$2E_2<E<E_c$	$(0,b_0)^{(b)},^{(b,d)}$ $[r_0,\infty]$**
Type 5	$E<E_2$	$(0,b_0)^{(b)},^{(b,d)}$ $[r_0,\infty]$**
	$E_2<E<E'_L$	$[r_{m0},r_{m1}]^{(c,d)}$, $[r_{m1},\infty]$**
	$E'_L<E<E_L$	$(0,r_{2c})$, (r_{2c},∞)*
	$E_L<E<E_c$	$(0,b_0)^{(b)},^{(b,d)}$ $[r_0,\infty]$**
All types	$E_c<E<3E_c$	$[r_{m0},r_{m1}]^{(c,d)}$, $[r_{m1},\infty]$**
	$3E_c<E<10^3E_c$	$(0,r_c)$, (r_c,∞)*
	$E>10^3E_c$	$(0,1)$, $(1,\infty)$*

grand approach infinite frequency.

Fortunately, an alternate technique is at our disposal, i.e., the use of r_m, the distance of closest approach, as a variable of integration in place of b. For an arbitrary function $G(b)$, the transformation is

$$\int db\, G(b) = \int dr_m \frac{db}{dr_m} G[b(r_m)]$$
$$= \int r_m\, dr_m\, [E-\phi(r_m)-\tfrac{1}{2} r_m\, \phi'(r_m)]$$
$$\times G\left[r_m\left(1-\frac{\phi(r_m)}{E}\right)^{1/2}\right]\Big/ Eb\ . \qquad \text{(E1)}$$

The use of r_m as integration variable has several advantages. The oscillations at orbiting are in part suppressed with the use of r_m because db/dr_m approaches zero as b approaches b_0 from above (but *not* from below). Also, b can be determined from r_m algebraically, which bypasses the root-finding difficulties discussed in Appendix B. There are also disadvantages; additional functional evaluations are required, the integration region for r_m with orbiting is discontinuous (though continuous for b), and the limits of integration must be found by a numerical root search (whereas, for b, the limits are simply zero and infinity).

O'Hara and Smith[3] employ both variables to exploit the special advantages of each. For $E<E_c$ the integral is split at b_0. In the lower interval b is used as the integration variable together with Eq. (23) which suppresses the oscillations at orbiting. For the upper interval, r_m is used and the integration variable is shifted and then inverted as follows:

$$\int_{r_0}^{\infty} dr_m\, G(r_m) = \int_0^{(r_0+1)^{-1}} dy_m\, y_m^{-2}\, G(y_m^{-1}-1)\ , \qquad \text{(E2)}$$

and, since this integrand happens to be peaked sharply at the upper end because the scattering angle, in magnitude, drops abruptly with b above orbiting, the transformation of Eqs. (21)–(23) is then used.

For energies immediately above E_c, where orbiting does not occur but there is a large negative minimum in the scattering angle [cf. Fig. 3(c)], O'Hara and Smith split the interval at the minimum angle point, defined as b_r and determined numerically, and use r_m for both subintervals. For larger energies the interval is split at r_c (Fig. 2), which is a convenient approximation to b_r and whose use avoids another root search, and employ b over both subintervals with simple inversion of the upper one [cf. Eq. (20)]. The procedure for very large energies has been addressed in Appendix A.

For the more complicated binary dynamics of the general HH potential, we follow closely the philosophy of O'Hara and Smith. Because of the many different possibilities our methods are most concisely displayed in tabular form, as shown[19] in Table VI. The integration variable is b for an interval listed in parentheses and r_m for one listed in square brackets. The superscripts denote suppression of the indicated end of that interval for the reason, (b), (c), or (d), explained in the discussion below Eq. (23). A single asterisk denotes inversion by Eq. (20), a double asterisk inversion by Eq. (E2).

The variables in Table VI have all been defined previously except for the following;

$$b_{av} = (b_0+b_2)/2\ , \qquad \text{(E3)}$$

$$r_{av} = r_m(b_{av}, E)\ , \qquad \text{(E4)}$$

$$b_{2c} = b_2(E_2)\ , \qquad \text{(E5)}$$

TABLE VII. Energy intervals for Chebyshev fits.

Potential	Intervals
Type 1 and Type 2, $E_1 \geq 0.8\,E_2$	(E_{min}, E_c), $(E_c, 10E_c)$, $(10E_c, E_{max})$
Type 3 and Type 2, $E_1 < 0.8\,E_2$	(E_{min}, E_2), (E_2, E_{av}), (E_{av}, E_c), $(E_c, 10E_c)$, $(10E_c, E_{max})$
Type 4	(E_{min}, E_L), (E_L, E_2), (E_2, E_{av}), (E_{av}, E_c), $(E_c, 10E_c)$, $(10E_c, E_{max})$
Type 5	(E_{min}, E_2), (E_2, E_L), (E_L, E'_{av}), (E'_{av}, E_c), $(E_c, 10E_c)$, $(10E_c, E_{max})$

$$r_{2c} = r_m(b_{2c}, E_2) \ , \tag{E6}$$

$$b'_{av} = (b_0 + b_{2c})/2 \ , \tag{E7}$$

$$r'_{av} = r_m(b'_{av}, E) \ , \tag{E8}$$

$$r_{m0} = r_m(0, E) \ , \tag{E9}$$

$$r_{m1} = r_m(b_r, E) \ , \tag{E10}$$

and for type 5 potentials

$$E'_L = \min(E_L, 2E_2) \ . \tag{E11}$$

The algorithm for type 1 potentials follows that of O'Hara and Smith, but with a few exceptions.[19] For some of the integrals with infinity as upper limit, O'Hara and Smith employ only positive Clenshaw–Curtis abscissas.[3] We believe this procedure is not warranted for certain potentials, as we explain elsewhere.[17] Hence, in the integrals of Table VI both positive and negative abscissas are always used.

An additional problem, peculiar to double orbiting, is that for type 2 and 3 potentials b_0 and b_2 may be so close that the maximum scattering angle between the two orbiting points, Fig. 3(c) is in absolute value several multiples of π. In such cases the integrand is so highly oscillatory that the methods of Table VI fail to converge, and it is preferable to treat $\cos\chi$, because of its extremely oscillatory nature, as a random variable, i.e., for $b_0 \approx b_2$,

$$\int_{b_0}^{b_2} b\,db(1 - \cos^l \chi) = \tfrac{1}{2}(b_2^2 - b_0^2)\langle 1 - \cos^l \chi\rangle \ , \tag{E12}$$

where $\langle\ \rangle$ denotes the average over a complete cycle in χ,

$$\langle 1 - \cos^l \chi\rangle = \frac{1}{2\pi}\int_0^{2\pi} d\chi(1 - \cos^l \chi) \ . \tag{E13}$$

This procedure is inspired by an interesting "random phase approximation" treatment of collision integrals.[20] Errors associated with use of Eq. (E12) should be negligible since, if $b_0 \approx b_2$, the interval from b_0 to b_2 contributes a very small part to the total integral. The criteria for use of Eq. (E12) in our program are that $(b_2 - b_0)/b_2$ be less than both 0.05 and 20 times the accuracy input. Its use should be infrequent and the program prints a message on the occasion that it is needed.

APPENDIX F: INTEGRATION OVER ENERGY

Equation (6) for the collision integral may be written as

$$\Omega^{(l,s)*} = (C_{ls}/2\pi)\int_0^\infty E^{s+1} e^{-E/kT}\, Q_l(E)\, dE \ , \tag{F1}$$

where

$$Q_l(E) = 2\pi\int_0^\infty b\,db(1 - \cos^l \chi) \ . \tag{F2}$$

In this manner the dynamical and statistical (or thermal) parts of the problem are separated. $Q_l(E)$ depends only on the dynamics of two-body collisions with relative total energy E. The only appearance of temperature is in the Boltzmann factor $\exp(-E/kT)$ of the energy integral.

The user typically calculates collision integrals for a particular potential and a list of N reduced temperatures; in our runs, typically, $N = 46$. Direct evaluation of Eqs. (F1) and (F2) would then require N three-dimensional numerical integrals, since χ must also be calculated numerically. However, the separation into dynamical and statistical parts makes possible an alternate procedure which saves considerable computer time.[3] The cross section $Q_l(E)$ can be fit to a Chebyshev polynomial series in E, and in the subsequent calculation of the energy integral, $Q_l(E)$ is taken from the fit rather than integrated directly. In practice it is most efficient to fit $\log Q_l$ versus $\log E$.

The Chebyshev fitting procedure[3] is closely related to the Clenshaw–Curtis quadrature, and has similar rules for accuracy inputs and error estimates. Construction of the fit is thus equivalent to performance of a small number of three-dimensional integrals, depending on the number of energy intervals required (see below). Once the fit is constructed, in effect N one-dimensional integrals are required. Considerable computation is saved and the time required is almost independent of N.

$Q_l(E)$ is required from a minimum energy E_{min} to a maximum energy E_{max}, which are determined from the extremal input temperatures and the extremal Clenshaw-Curtis abscissas which can be used in Eq. (F1). O'Hara and Smith[3] divide the full energy range into three intervals such that $\log Q$ is a smooth function of $\log E$ over each interval and the Chebyshev series thus converges rapidly.

With the more complicated binary collision dynamics of the general HH potential, $Q_l(E)$ is not as simple a function of E and, for the higher types, more energy intervals are required. The choice of intervals is somewhat arbitrary, but we have found that the division listed in Table VII works well.[21] All variables in this table have been defined previously except

$$E_{av} = (E_2 E_c)^{1/2} \ , \tag{F3}$$

$$E'_{av} = (E_L E_c)^{1/2} \ . \tag{F4}$$

The actual integration over E is straightforward. Following O'Hara and Smith,[3] we split the integration range at $E = s + 1$, which corresponds approximately to

the maximum of the integrand. The lower integral is computed directly [cf. Eq. (19)] and the upper integral is computed similarly after a simple inversion [cf. Eq. (20)].

[1]J. O. Hirschfelder, C. F. Curtiss, and R. B. Bird, *Molecular Theory of Gases and Liquids* (Wiley, New York, 1954).

[2]F. J. Smith and R. J. Munn, J. Chem. Phys. **41**, 3560 (1964).

[3]H. O'Hara and F. J. Smith, J. Comput. Phys. **5**, 328 (1970).

[4]H. O'Hara and F. J. Smith, Comput. Phys. Commun. **2**, 47 (1971).

[5]M. Klein, H. J. M. Hanley, F. J. Smith, and P. Holland, Natl. Bur. Stand. (U.S.), Monogr. Natl. Stand. Ref. Data Ser., Natl. Bur. Stand. 47 (1974).

[6]H. J. M. Hanley and M. Klein, J. Phys. Chem. **76**, 1743 (1972).

[7]H. M. Hulburt and J. O. Hirschfelder, J. Chem. Phys. **9**, 61 (1941); **35**, 1901 (1961).

[8]L. Biolsi, J. Geophys. Res. **83**, 2476 (1978); L. Biolsi and K. J. Biolsi, *ibid.* **84**, 5311 (1979).

[9]P. M. Holland, L. Biolsi, and J. C. Rainwater (to be published).

[10]L. Biolsi, J. C. Rainwater, and P. M. Holland, J. Chem. Phys. **77**, 448 (1982).

[11]P. M. Morse, Phys. Rev. **34**, 57 (1929). The Morse potential is more commonly expressed in the form $\phi(r) = \epsilon\{\exp[-2c(r-r_e)/\sigma] - 2\exp[-c(r-r_e)/\sigma]\}$ which is equivalent to Eq. (5) if $d = r_e/\sigma$ and $a = cd$.

[12]R. S. Mullikan, J. Phys. Chem. **41**, 5 (1937).

[13]T. Kihara, *Intramolecular Forces* (Wiley, New York, 1978).

[14]J. C. Rainwater, J. Chem. Phys. **71**, 5171 (1979).

[15]J. F. Ely and H. J. M. Hanley, Mol. Phys. **30**, 565 (1975).

[16]C. W. Clenshaw and A. R. Curtis, Numer. Matl. **2**, 197 (1960).

[17]J. C. Rainwater, J. F. Ely, and H. J. M. Hanley, (to be published).

[18]Z. Kopal, *Numerical Analysis* (Wiley, New York, 1955), p. 36.

[19]The algorithm for type 1 potentials follows that described in Ref. 3 with the following exceptions. In Ref. 3 the upper integral with r_m as the variable is performed in a manner equivalent to replacing the shift and inversion of Eq. (E2) with the simple inversion of Eq. (20). The upper limit of the second energy region is $10E_c$, not $3E_c$. In the third energy region the b integral is split at b_r, not r_c. Finally, in the upper interval the split is at b', not 1.0 (see Appendix A). Except for the latter, these changes have been incorporated into the published program of O'Hara and Smith (Ref. 4).

[20]G. C. Maitland, E. A. Mason, L. A. Viehland, and W. A. Wakeham, Mol. Phys. **36**, 797 (1978).

[21]When an interval in Table VII is bounded by E_c, E_2, or E_L, the actual energy used is very slightly less than the indicated one so that the calculation of a singular integral is avoided.